Identifying the Failure-Tolerant Workspace Boundaries of a Kinematically Redundant Manipulator

Rodney G. Roberts[†], Rodrigo S. Jamisola, Jr.[‡], and Anthony A. Maciejewski[‡]

Abstract— In addition to possessing a number of other important properties, kinematically redundant manipulators are inherently more tolerant to locked-joint failures than non-redundant manipulators. However, a joint failure can still render a kinematically redundant manipulator useless if the manipulator is poorly designed or controlled. This paper presents a method for identifying a region of the workspace of a redundant manipulator for which task completion is guaranteed in the event of a locked-joint failure. The existence of such a region, called a *failure-tolerant workspace*, will be guaranteed by imposing a suitable set of artificial joint limits prior to a failure. Conditions are presented that characterize end-effector locations in this region. Based on these conditions, a method is presented that identifies the boundaries of the failure-tolerant workspace. Optimized failure-tolerant workspaces for a three degree-of-freedom planar robot are presented.

I. INTRODUCTION

Kinematically redundant manipulators have a number of advantages over non-redundant manipulators including the potential for obstacle avoidance and greater dexterity. In this work, we consider the important advantage of fault tolerance. Failures can cause unnecessary delays due to repairs and can even pose a significant danger during task execution. Since a kinematically redundant manipulator has more joints than are required for its specified task, it is possible that the manipulator can still perform its required task even if it suffers a joint failure. Fault tolerance is particularly important for manipulators operating in hazardous or remote environments such as in space exploration [1] and nuclear waste disposal [2]. A number of studies have been dedicated to the assessment [3] and analysis [4], [5] of robot reliability. Other studies related to enhancing a robot's tolerance to failure include work on layered failure tolerance control [6], failure tolerance by trajectory planning [7], kinematic failure recovery [8] and manipulators specifically designed for fault tolerance [9]. In this article, a motion planning technique is proposed that uses an a priori strategy so that joint failures can be gracefully accommodated.

One approach to guaranteeing fault tolerance is to add enough kinematic redundancy to compensate for a locked-joint failure. It was shown in [10] that to insure the fault tolerance of a manipulator operating in an m-dimensional workspace, $m + 2$ joints are required if the joint space is unconstrained. However, adding too much kinematic redundancy is typically undesirable and actually makes the robotic system more likely to fail. A more practical problem is to improve the fault tolerance of an existing robot geometry. This can be accomplished by introducing joint constraints.

By judiciously choosing suitable joint constraints, one can significantly increase the manipulator's fault-tolerant workspace even if the manipulator only has one degree of redundancy. In [11] failure-tolerant workspaces that contain prescribed end-effector locations were identified by using bounding boxes in the configuration space that enclose self-motion manifolds corresponding to selected end-effector locations. The intersection of the bounding boxes determine a set of artificial joint limits that will guarantee reachability between the specified task points after a joint failure.

The approach that we introduce here is also based on the idea of using artificial joint limits. However, rather than guaranteeing reachability between specified workspace points, this work focuses on finding the boundaries of a failure-tolerant workspace. Artificial joint limits provide the necessary constraints prior to a failure to avoid those configurations where a failure can have a detrimental effect. A proper choice of these limits can result in a larger failure-tolerant workspace. Thus, the crux of our approach is that making a compromise in the pre-failure workspace by introducing joint limits can help insure a suitable post-failure workspace. It is assumed that once a joint failure occurs, that joint is immediately locked. In this case, the artificial joint limits are released and the remaining healthy joints are allowed to freely move within their physical joint limits.

In the next section, the fault-tolerant workspace problem is mathematically formulated. In Section III, the problem of identifying the pre-failure workspace is described. The boundaries of this workspace are identified by kinematic singularities and joint-limit singularities. New techniques for identifying workspace boundaries due to multiple joint limits are described. In Section IV, conditions for the fault-tolerant workspace are given. These conditions are used in Section V to identify potential boundaries for the fault-tolerant workspace. The technique is illustrated with an example in Section VI, and conclusions appear in Section VII.

[†]R. G. Roberts is with the Department of Electrical and Computer Engineering, Florida A&M-Florida State University, Tallahassee, FL 32310-6046, USA (e-mail: rroberts@eng.fsu.edu)

[‡]R. S. Jamisola, Jr. & A. A. Maciejewski are with the Department of Electrical and Computer Engineering, Colorado State University, Fort Collins, CO 80523-1373, USA (e-mails: {r.jamisola, aam}@colostate.edu)

II. PROBLEM FORMULATION

Let the kinematic function mapping the joint space $\mathcal{C} \subset \mathbb{R}^n$ to the workspace $\mathcal{W} \subset \mathbb{R}^m$ be denoted by $\mathbf{f} : \mathcal{C} \to \mathcal{W}$. In this work, we will assume that the configuration space $\mathcal{C}$ has the form $\mathcal{C}_B = B_1 \times \cdots \times B_n$. If joint i has no physical joint limits, $B_i = \mathbb{R}$, and if joint i does have physical joint limits, $B_i = [\underline{b}_i, \bar{b}_i]$ where $\underline{b}_i < \bar{b}_i$. Initially we introduce artificial limits for each joint so that the i-th joint $q_i \in A_i = [\underline{a}_i, \bar{a}_i]$. If it can be safely assumed that joint i will not fail then we can set $A_i = B_i$. The set $\mathcal{C}_A = A_1 \times \cdots \times A_n$ denotes the region of the configuration space corresponding to the artificial joint limits. The joint space prior to a failure is then simply $\mathcal{C}_A$. Once a locked-joint failure occurs, the artificial joint limits are released and the robot is constrained to operate on a failure-induced hyperplane. This of course has a significant impact on the resulting reachable workspace. There are generally end-effector locations that were reachable prior to the failure that are no longer reachable after a failure. There may also be areas of the workspace that were formerly unreachable but that, in spite of the locked joint, become reachable after releasing the artificial joint limits of the non-failed joints. The *fault-tolerant workspace* is defined as the part of the workspace that is reachable prior to and after any single locked-joint failure where the joint failure can occur at any configuration in $\mathcal{C}_A$.

To illustrate the significance of the fault-tolerant workspace, consider a planar 3R manipulator with equal length links. Without artificial or physical joint limits, the fault-tolerant workspace is quite small. This can be clearly seen in Fig. 1, where two configurations corresponding to the same end-effector location on the unit circle are shown. While the first configuration is relatively fault tolerant to a locked-joint failure, the second configuration is fault intolerant to joint 3 being locked, in which case the end effector is constrained to remain on the dashed circle shown in the figure. In fact, it was shown in [11] that this unit circle is the only region of the workspace that is guaranteed to be reachable following any possible locked-joint failure. However, it will be shown in Section VI that the fault-tolerant workspace can be significantly increased by simply enforcing artificial joint limits that can be released after a failure.

In some cases, only certain joints are prone to failures. Let the *failure index set* $\mathbf{F} \subset \{1, 2, \ldots, n\}$ denote the joint labels of the failure-prone joints. We will assume that those joints that are not contained in $\mathbf{F}$ will remain healthy throughout the robot's mission. Our goal then is to determine the fault-tolerant workspace corresponding to at most one locked-joint failure where any joint $i \in \mathbf{F}$ can fail. Mathematically, this problem can be formulated in the following way. Prior to a joint failure, the robot's operating configuration space is $\mathcal{C}_A$ and the pre-failure workspace is given by

$$\mathcal{W}_0 = \mathbf{f}(\mathcal{C}_A) = \{\mathbf{x} = \mathbf{f}(\mathbf{q}) \mid \mathbf{q} \in \mathcal{C}_A\}. \quad (1)$$

If the i-th joint is locked at $q_i = \theta_i$ and the remaining artificial joint limits are released, the resulting reduced
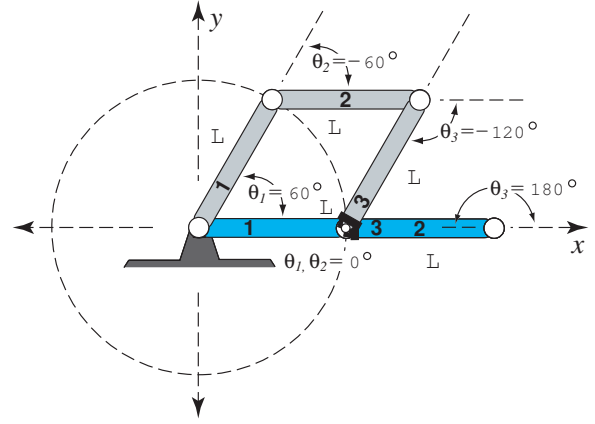

Fig. 1. Two configurations of a planar 3R robot with equal link lengths of L meters. The configurations shown are from an infinite family of configurations resulting in the end-effector position $[L, 0]^T$. The first configuration, $\boldsymbol{\theta} = [60°, -60°, -120°]^T$, is fault tolerant but the second configuration, $\boldsymbol{\theta} = [0°, 0°, 180°]^T$, is fault intolerant to a locked-joint failure in the third joint as this will restrict the end effector to remain on the circle shown regardless of the values of the remaining two healthy joints.

configuration space is given by

$$^i\mathcal{C}(\theta_i) = \{\mathbf{q} \in \mathcal{C}_B \mid q_i = \theta_i\}. \quad (2)$$

Geometrically, one can consider $^i\mathcal{C}(\theta_i)$ to be the intersection of the hyperplane given by $q_i = \theta_i$ with the feasible configuration space $\mathcal{C}_B$. Because the artificial joint limits were enforced prior to the failure, we have that $\underline{a}_i \leq \theta_i \leq \bar{a}_i$. It is assumed that the failure can occur anywhere in this interval and the joint is locked at that configuration. Hence, the guaranteed workspace following a locked-joint failure of joint i subject to the artificial joint limits is

$$\mathcal{W}_i = \bigcap_{\underline{a}_i \leq \theta_i \leq \bar{a}_i} \mathbf{f}(^i\mathcal{C}(\theta_i)). \quad (3)$$

The fault-tolerant workspace is then the intersection of the pre-failure workspace $\mathcal{W}_0$ and the various post-failure fault-tolerant workspaces $\mathcal{W}_i$, $i \in \mathbf{F}$:

$$\mathcal{W}_F = \bigcap_{i \in F \cup \{0\}} \mathcal{W}_i. \quad (4)$$

Our goal is to determine $\mathcal{W}_F$.

Unfortunately, finding $\mathcal{W}_F$ directly is generally impossible, so the approach taken here will be to identify necessary conditions for its boundaries. Recall that a boundary point of a subset $\mathcal{S}$ of $\mathbb{R}^m$ is a point $\mathbf{x} \in \mathbb{R}^m$ such that every open neighborhood of $\mathbf{x}$ contains at least one point in $\mathcal{S}$ and at least one point not in $\mathcal{S}$. Although the boundary of a general point set can be quite complicated, the boundary sets considered in this work are simple and correspond to simple curves or hyper-surfaces, depending on the dimension of the workspace. These boundaries are determined by first identifying candidate boundary sets. These candidate boundary sets correspond to a limitation in the manipulator's ability to move its end effector arbitrarily. In particular, the candidate workspace boundaries prior to a failure are related to the concepts of kinematic singularities and joint-limit

singularities. In the next section, we will describe how one can identify these candidate boundaries. Conditions are then introduced in Section IV and are subsequently applied in Section V to identify the fault-tolerant workspace boundaries.

III. IDENTIFYING THE PRE-FAILURE WORKSPACE BOUNDARIES

Before developing criteria for identifying the fault-tolerant workspace boundary, we discuss the problem of identifying the workspace boundary of a healthy robot without any failures. These boundaries are located by identifying two types of singularities: kinematic singularities and joint-limit singularities.

The local motion of the end effector is characterized by the Jacobian equation

$$\mathbf{v} = J\dot{\mathbf{q}} \tag{5}$$

where $\mathbf{v}$ denotes the end-effector velocity, $\dot{\mathbf{q}}$ denotes the joint velocity, and J denotes the manipulator Jacobian. If the manipulator Jacobian has full rank and the joints are unconstrained, then the end effector can move locally in any direction. In this case, the end effector is at an interior point of the workspace. If the manipulator Jacobian does not have full rank, i.e., if the robot is in a *kinematic singularity*, then the end effector does not locally have full motion control. This occurs for example at a reach singularity. Note that not all kinematic singularities correspond to workspace boundaries. However, since the workspace boundaries of a manipulator without joint limits can only occur at kinematic singularities, kinematic singularites can be used to identify candidate workspace boundaries.

When the manipulator has joint limits, the columns of the manipulator Jacobian corresponding to the constrained joints can only contribute in one direction (a positive amount if the joint is in a lower limit and a negative amount if the joint is in an upper limit). In some cases, this may cause the loss of full end-effector motion even if the manipulator is not in a kinematic singularity. The joint configuration in this case is said to be a *joint-limit singularity* (the term *semi-singularity* is also used [13]). A workspace boundary implies that the manipulator is either in a kinematic singularity or a joint-limit singularity. This observation can be used to find the workspace boundaries of the manipulator, but once again, it is important to note that the end-effector location corresponding to a kinematic singularity or a joint-limit singularity is not necessarily a boundary point.

Kinematic singularities are relatively easy to find; they are simply those configurations where the manipulator Jacobian does not have full rank. For a kinematically redundant manipulator these configurations are characterized by $\det(JJ^T) = 0$. This is further simplified for the case of a single degree of redundancy by the fact that $\det(JJ^T) = \|\mathbf{n}_J\|_2^2 = n_{J1}^2 + \cdots + n_{Jn}^2$ where $\mathbf{n}_J$ is the canonical null vector of J, i.e., the null vector obtained by taking the equivalent of the cross product of the rows of J. Hence, the kinematic singularities are those configurations for which each element

n_{Ji} of $\mathbf{n}_J$ is zero. This is easily illustrated for a planar 3R manipulator, which has as its canonical null vector

$$\mathbf{n}_J = \begin{bmatrix} l_2 l_3 \sin\theta_3 \\ -l_2 l_3 \sin\theta_3 - l_1 l_3 \sin(\theta_2 + \theta_3) \\ l_1 l_2 \sin\theta_2 + l_1 l_3 \sin(\theta_2 + \theta_3) \end{bmatrix} \tag{6}$$

where l_i denotes the length of the i-th link and θ_i denotes the angle of the i-th joint. The kinematic singularities are precisely those configurations $\boldsymbol{\theta}$ where each component of (6) is zero. From the first component of (6) it is clear that θ_3 must be a multiple of π and, since the sum, $-l_1 l_3 \sin(\theta_2 + \theta_3)$, of the first two components of (6) is zero, it follows that $\theta_2 + \theta_3$ is also a multiple of π. Hence the kinematic singularities of the general planar 3R is given by $(\theta_2, \theta_3) = (k\pi, l\pi)$ where k and l are integers. Physically, the links are completely extended or folded back or a combination of the two.

Identifying joint-limit singularities is a more challenging problem, particularly when more than one joint is at its limit. As with kinematic singularities, joint-limit singularities are characterized by a local loss of full end-effector motion. In this case, full motion control is lost because one or more joints are at their limits. To more clearly see the reason for the problem, we note that pseudoinverse control $\dot{\mathbf{q}} = J^+\mathbf{v}$ is typically insufficient for full end-effector control when one or more joints are at their limit. Indeed, if the end-effector velocity $\mathbf{v}$ is feasible under pseudoinverse control where at least one constrained joint has a non-zero joint velocity moving that joint away from its limit, then the end-effector velocity $-\mathbf{v}$ would not be feasible as it would require the constrained joint to move past its limit. In such cases, one must rely on the null space to add enough joint velocity to meet the required joint velocity constraints while still achieving the desired end-effector motion.

It can be shown that if a manipulator has a single degree of redundancy and is not in a kinematic singularity, then the family of joint velocities that result in the end-effector velocity $\mathbf{v}$ is given by

$$\dot{\mathbf{q}} = J^+\mathbf{v} + \alpha\mathbf{n}_J \tag{7}$$

where α is an arbitrary scalar. In order for (7) to be feasible given the joint-limit conditions, the components corresponding to the actively constrained joints must have the appropriate sign, i.e., if joint i is at its upper (lower) limit, the joint velocity $\dot{q}_i$ must be non-positive (non-negative). If the i-th component of $\mathbf{n}_J$ is nonzero, then choosing an appropriate value for α will allow (7) to be feasible. On the other hand, if the i-th component of $\mathbf{n}_J$ is zero, then no amount of the null vector can be added in (7) to adjust the sign of the $\dot{q}_i$ and consequently, certain end-effector velocities will not be possible. If two or more joints are at their limits, then the relative directions of the columns of the manipulator Jacobian must be examined. For example, if joints i and j $(i \neq j)$ are at their upper limits, then the null space term can compensate for the joint limits provided that n_{Ji} and n_{Jj} are nonzero and of the same sign. Otherwise, certain end-effector velocities cannot be achieved. However, if joint

i is at its upper limit and joint j is at its lower limit, arbitrary end-effector velocities can be achieved if and only if n_{Ji} and n_{Jj} are nonzero and of the opposite sign. The generalization to more joints being at their limits is obvious. Similar results hold for robots with higher degrees of redundancy, e.g., if two joints are at their upper limits, there must be a vector of the null space of J for which the corresponding components are nonzero and of the same sign. Of course, this is easier to determine when there is only a single degree of redundancy. More details on the multiple degree-of-redundancy case can be found in [14].

There are a significant number of cases to check when identifying potential joint-limit singularities when multiple joints are at their limits. Consider an n degree-of-freedom manipulator where each joint has an upper and lower limit. One first needs to check for the kinematic singularities of the robot. One can then check the cases when precisely one joint is at one of its limits. There are n joints and for each joint we must consider its upper and lower limit. There are then $2n$ such cases to consider for having a single joint at its limit. Next, one can check the cases when there are precisely two joints at a limit. In this case there are $\binom{n}{2}$ combinations of two joints to consider of which there are four subcases to consider based on which combination of upper/lower joint limits are evaluated. This results in $\binom{n}{2}2^2$ cases. More generally, there are $\binom{n}{k}2^k$ cases to consider when evaluating scenarios with precisely k joints at their limits. Adding all of these cases together, we have a total of 3^n cases to check. The value of this quantity also follows from the fact that there are three cases for each individual joint: the joint is at its upper limit, lower limit, or in between these limits. Hence, there are $3^7 = 2187$ cases to consider for a fully spatial 7R manipulator if each joint has an upper and lower limit. Each of these cases would need to be considered when identifying kinematic and joint-limit singularities. In the case of a 7R anthropomorphic arm, configurations for which the elbow joint is at its limit are clearly joint-limit singularities due to the critical importance of the elbow in moving the position of the wrist center.

IV. CONDITIONS FOR FAILURE TOLERANT WORKSPACE LOCATIONS

Whether or not a given end-effector location is in the fault-tolerant workspace is completely determined by its pre-image, i.e., the family of configurations corresponding to that workspace location. The pre-image of a workspace location $\mathbf{x} \in \mathcal{W}$ is the set

$$\mathbf{f}^{-1}(\mathbf{x}) = \{\mathbf{q} \in \mathcal{C}_B \mid \mathbf{f}(\mathbf{q}) = \mathbf{x}\}. \qquad (8)$$

The reachability of the end-effector location $\mathbf{x}$ after a locked-joint failure has occurred is determined by whether or not the joint value of the locked joint falls within that individual joint range of the set $\mathbf{f}^{-1}(\mathbf{x})$. In particular, the end-effector location $\mathbf{x}$ is still reachable when joint i is locked at $q_i = \theta_i$ if and only if θ_i is contained in the projection of $\mathbf{f}^{-1}(\mathbf{x})$ onto the i-th axis. The projection of a set $\mathbf{S} \subset \mathbb{R}^n$ is given

by

$$P_i[\mathbf{S}] = \{s_i \mid \mathbf{s} = \begin{bmatrix} s_1 & s_2 & \cdots & s_n \end{bmatrix}^T \in \mathbf{S}\}. \qquad (9)$$

Note that $P_i[\mathbf{S}]$ is a subset of $\mathbb{R}$ that can be thought of as the projection of $\mathbf{S}$ onto the i-th axis. Thus the end-effector location $\mathbf{x}$ can be reached after a locked-joint failure $q_i = \theta_i$ if and only if $\theta_i \in P_i[\mathbf{f}^{-1}(\mathbf{x})]$.

We can now formally state the characterizing conditions for the fault-tolerant workspace $\mathcal{W}_F$. A workspace region is failure tolerant to a single failure in joint $i \in \mathbf{F}$ for a given $\mathcal{C}_A$ and a given $\mathcal{C}_B$ if and only if the following two conditions hold:

Condition 1. Reachability prior to a failure: For any $\mathbf{x} \in \mathcal{W}_F$,

$$\mathcal{C}_A \cap \mathbf{f}^{-1}(\mathbf{x}) \neq \emptyset. \qquad (10)$$

Condition 2. Reachability after a failure: For any $\mathbf{x} \in \mathcal{W}_F$,

$$A_i \subset P_i[\mathbf{f}^{-1}(\mathbf{x})] \text{ for } i \in \mathbf{F}. \qquad (11)$$

Condition 1 is simple enough; it merely says that any $\mathbf{x} \in \mathcal{W}_F$ should be reachable prior to a failure, i.e., there is at least one configuration in the pre-image of $\mathbf{x}$ that is contained in the pre-failure configuration space $\mathcal{C}_A$. Equation (10) is equivalent to $\mathbf{x} \in \mathcal{W}_0$. Condition 2 is somewhat more complicated. In order for the manipulator to be capable of reaching a workspace configuration $\mathbf{x}$ following a locked-joint failure in joint i that can occur at any angle within its specified artificial limits, the pre-image of $\mathbf{x}$ must have at least one configuration whose i-th component is equal to that joint value. Condition 2 insures that this is true for all joint values within the individual artificial joint limits for each failure-prone joint. If Conditions 1 and 2 hold, the end-effector location $\mathbf{x}$ is failure tolerant to a locked-joint failure of any joint in the set $\mathbf{F}$. Equation (11) is equivalent to $\mathbf{x} \in \mathcal{W}_i$ for $i \in \mathbf{F}$.

V. IDENTIFYING THE FAULT TOLERANT WORKSPACE BOUNDARIES

In Section II, we formulated the problem of identifying the fault-tolerant workspace in terms of the intersection of the pre-failure workspace with the intersection of a continuous family of images of hypersurfaces ${}^i\mathcal{C}(\theta_i)$ as θ_i is varied over A_i, $i \in \mathbf{F}$. Although mathematically correct, this approach is not a feasible method for identifying the fault-tolerant workspace. In Section IV, characterizing conditions based on the pre-images of workspace locations were given. Since closed form expressions for pre-images are difficult if not impossible to obtain, this approach is also not a feasible method for determining the fault-tolerant workspace. Instead, we will use these conditions to identify candidate boundaries of the fault-tolerant workspace.

Based on the two conditions introduced in Section IV, we can develop necessary conditions for identifying the boundaries of the fault-tolerant workspace $\mathcal{W}_F$. Condition 1 relates to the workspace prior to a failure, and the techniques for finding its workspace boundaries were already developed

in Section III. Condition 2 can be used to identify additional potential boundaries related to a locked-joint failure. Once all of the potential boundaries have been identified, one can readily test these candidate boundaries to determine the real boundaries of the fault-tolerant workspace.

Consider a manipulator operating within the prescribed artificial joint limits. When a given location $\mathbf{x}$ is within the failure-tolerant workspace, its pre-image satisfies Condition 2 for $i \in \mathbf{F}$. Our goal is to identify those workspace locations that form the boundary between where Condition 2 is satisfied and where it is violated, i.e., a potential boundary of the fault-tolerant workspace. This can occur in two ways: (case I) the projection of the preimage for this workspace location fails to contain an endpoint of A_i or (case II) the projection of its preimage becomes disjoint within A_i. We will systematically identify the complete set of these potential boundaries and introduce a procedure to extract the true boundary.

While the formulation of Condition 2 is based on the concept of a pre-image, when identifying boundaries, it is more convenient to work with self-motion manifolds. The *self-motion manifolds* of an end-effector location $\mathbf{x}$ are the disjoint, connected subsets of the pre-image $\mathbf{f}^{-1}(\mathbf{x})$. For a manipulator with r degrees of redundancy,

$$\mathbf{f}^{-1}(\mathbf{x}) = \bigcup_{i=1}^{N} \mathcal{M}_i \quad (12)$$

where $\mathcal{M}_i$ is the i-th r-dimensional self-motion manifold in the inverse kinematic pre-image such that $\mathcal{M}_i \cap \mathcal{M}_j = \emptyset$ when $i \neq j$ and N is the number of self-motion manifolds [12]. The term self-motion is meant to suggest the fact that as the robot moves along a self-motion manifold in the joint space, the end-effector location remains fixed so that the robot only moves itself and not an object located at the end effector.

When identifying the workspace boundaries, we will at times examine the minimum and maximum values of the different joint variables θ_i on the self-motion manifolds. For manipulators with a single degree of redundancy, the self-motion manifolds are smooth one-dimensional curves whose tangent vector is given by the null vector $\mathbf{n}_J$. Consequently, at minimum and maximum values of θ_i along the self-motion curve, we have $n_{Ji} = 0$. For manipulators with higher degrees of redundancy, the tangent space of the self-motion is given by the null space of the manipulator Jacobian.

We will now consider how to evaluate the potential boundaries characterized by case I and II. Case I has two subcases (a) and (b) that are illustrated in Figs. 2 and 3, respectively. Fig. 2 illustrates the subcase I(a) when the violation occurs inside $\mathcal{C}_B$. In this case, the self-motion manifold is tangent to the hyperplane corresponding to the artificial joint limit for joint i. When this occurs, $n_{Ji} = 0$. Thus, setting q_i to an artificial joint limit and solving for the remaining joints subject to the constraint $n_{Ji}(\mathbf{q}) = 0$ gives candidate joint configurations that may correspond to boundary points of the fault-tolerant workspace. One can

see from Fig. 2 that, in some sense, this can be viewed as an optimization problem in which one looks for extremal values of q_i along a self-motion manifold and those self-motion manifolds where these extremal values happen to occur on a hyperplane corresponding to an artificial joint limit are identified as possibly corresponding to a potential fault-tolerant workspace boundary.

In case I(b), illustrated in Fig. 3, the violation of Condition 2 occurs because the self-motion manifold exits $\mathcal{C}_B \subset \mathbb{R}^n$ before the projection of the self-motion onto the i-th axis can cover A_i so that the self-motion manifold cannot be reached if joint i is locked at the endpoint of A_i subject to the physical requirements that the manipulator must operate within $\mathcal{C}_B$. This case is characterized by the failure prone joint i being at an endpoint of A_i and some other joint $j \neq i$ being at an endpoint of B_j, where once again B_j is the set of joint values that are within the physical limits of joint j. In terms of a constrained optimization problem, Fig. 3 depicts a self-motion manifold for which the i-th component is maximized subject to the constraint $\mathbf{q} \in \mathcal{C}_B$ where at least one of the constraints (in this case, the constraint on joint j) is active.

Case II also contains two subcases, (a) and (b) that are illustrated in Figs. 4 and 5, respectively, where Condition 2 fails within the interior of A_i. Fig. 4 illustrates the case when the self-motion manifold exits $\mathcal{C}_B$ at a point where the manifold's projection is in the interior of A_i. Consequently, there are self-motion manifolds arbitrarily near the self-motion manifold in Fig. 4 that come outside of $\mathcal{C}_B$ so that their projections onto the i-th axis are disconnected inside A_i.

In case II(b), illustrated in Fig. 5, Condition 2 is violated in the interior of A_i where the failure occurs in the interior of $\mathcal{C}_B$ rather than at its boundary. This corresponds to a sudden change in the topological nature of the self-motion manifolds where the preimage becomes disconnected. In this case, the changes in topology are identified by co-regular surfaces [12] and the candidate boundaries are given by the images of the kinematic singularities of the robot.

Now that the set of candidate boundaries have been determined, our goal is to extract the true boundary. This is done by first determining if there are any intersections between the potential boundaries. These intersections are easily determined by checking to see if any points simultaneously satisfy multiple potential boundary conditions. The potential boundaries are then segmented into simple non-intersecting curves. Each of these curves is then checked to see if it satisfies Condition 2. Note that this can be efficiently done by selecting any convenient point along the curve. This is true because if one point on a simple potential boundary curve satisfies Condition 2, then the entire curve must satisfy Condition 2. Finally, all simple potential boundary curves that satisfy Condition 2 are checked to determine whether they are true boundaries or if they simply lie entirely within the fault-tolerant workspace. This is done by selecting two points that are perpendicular to a tangent of the potential boundary but lie on opposite sides. If only one of these
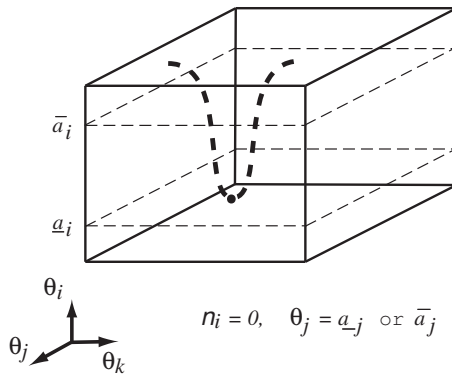
Fig. 2. An example of a self-motion manifold on the verge of violating Condition 2 at an endpoint of $A_i = [\underline{a}_i, \bar{a}_i]$. Arbitrarily near this self-motion manifold are self-motion manifolds that rise above the hyperplane $q_i = \underline{a}_i$, indicating that the corresponding end-effector location may not be within the fault-tolerant workspace. Self-motion manifolds that dip below the same hyperplane can also be found arbitrarily near the self-motion manifold shown in the figure. Hence, the corresponding end-effector location may be a boundary point of the fault-tolerant workspace. Since the self-motion manifold is tangent to the hyperplane, it follows that $n_{Ji} = 0$ when the self-motion manifold touches the hyperplane given by $q_i = \underline{a}_i$.
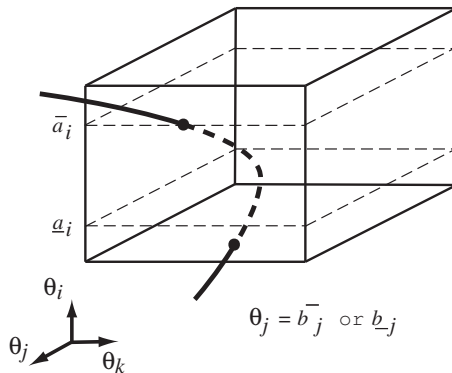

Fig. 4. An example of a self-motion manifold on the verge of violating Condition 2 at an interior point of A_i. The self-motion manifold is tangent to the j-th physical joint limit constraint so that $n_{Jj} = 0$. The corresponding end-effector location may be a boundary point of the fault-tolerant workspace as there are nearby self-motion manifolds that appear within $\mathcal{C}_B$ satisfying Condition 2, but there are also self-motion manifolds arbitrarily close by which come out of $\mathcal{C}_B \subset \mathbb{R}^n$, violating Condition 2 in the interior of $A_i = [\underline{a}_i, \bar{a}_i]$.

Fig. 3. Another example of a self-motion manifold on the verge of violating Condition 2 at an endpoint of $A_i = [\underline{a}_i, \bar{a}_i]$. The corresponding end-effector location may be a boundary point of the fault-tolerant workspace. In this case, there will be similar self-motion manifolds arbitrarily close by that fail Condition 2 as they exit the configuration space $\mathcal{C}_B \subset \mathbb{R}^n$ below the hyperplane given by $\theta_i = \bar{a}_i$. On the other hand, there will also be other self-motion manifolds arbitrarily close by that exit in such a way that Condition 2 is satisfied.

Fig. 5. An example of a portion of the configuration space containing a self-motion manifold that is not co-regular. The intersecting lines represent a set of joint values resulting in the same end-effector location. The configuration at the intersection is a kinematic singularity. Such configurations are associated with a fundamental change in the topology of the configuration space and may indicate a boundary point corresponding to a violation of Condition 2 at an interior point of A_i.

points satisfies Condition 2, then this portion of the potential boundary is a portion of the true fault-tolerant workspace boundary. The collection of all such curves that satisfy this last check form the complete connected boundary of the fault-tolerant workspace.

VI. AN ILLUSTRATIVE EXAMPLE

This section presents a simple example to illustrate the application of the algorithm discussed in the previous section. To simplify the visualization of the results, a planar 3-DOF robot is used, first constraining the link lengths to be equal and then determining an optimal ratio for the link lengths that maximizes the fault-tolerant workspace. In both cases there are no physical limits on the joint values.

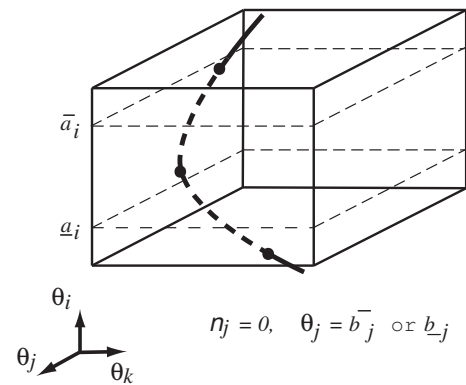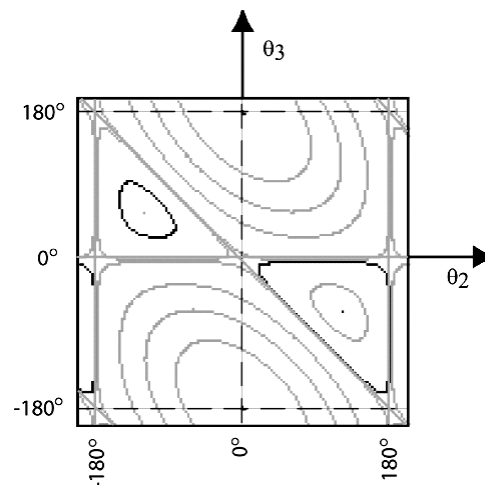The results of an optimization of the fault-tolerant workspace for the equal link length case are shown in Fig. 6, where the symbol $\mathcal{B}_T$ is used to denote the tangent potential boundary, and the symbol $\mathcal{B}_C$ is used to denote the co-regular potential boundary. Because physical joint limits are not considered, there are no tangent potential boundaries in this example.

If the constraint of equal link lengths is removed, then the area of the fault-tolerant workspace can be increased (see Fig. 7). In contrast to the equal link length case, the joint one failure workspace now contains a void. It is bounded by two tangent potential boundaries, $\mathcal{B}_T$'s, and two co-regular potential boundaries, $\mathcal{B}_C$'s. While it is natural to think that this void in the prefailure workspace is undesirable, this
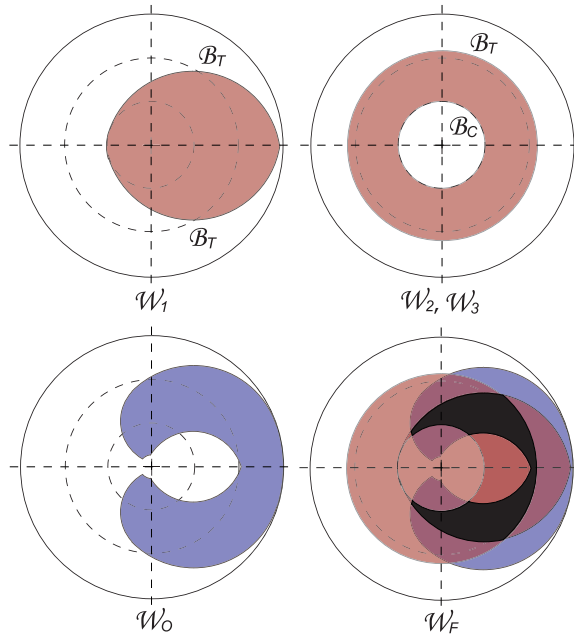
ratio of link lengths actually increases the value of $A_{\mathcal{W}_F}$ as compared to the equal link case. This is partially due to the fact that the void due to the internal singularity does not have any effect on the final fault-tolerant workspace. Thus the resulting $A_{\mathcal{W}_F}$ has a 4.2% increase over the equal link length case.

VII. CONCLUSIONS

This paper presented an approach for identifying the boundary of the fault-tolerant workspace of a manipulator. This approach is based on the evaluation of a small set of simple conditions based on the configuration space. By identifying the boundary, one can avoid an exhaustive evaluation of all potential fault-tolerant workspace locations. These conditions for potential fault-tolerant workspace boundaries also facilitate the optimization of the workspace based on manipulator design parameters. While the robot geometry and the degree of redundancy have a significant impact on the graceful degradation in the performance of a robot after a failure, our work has shown that it is critical to select a judicious set of artificially imposed joint limits prior to a failure.

Fig. 6. This figure illustrates the computation of an optimal fault-tolerant workspace for a 3-DOF planar robot with equal unit link lengths. The potential boundaries are shown for the three possible joint failures as well as for the artificially constrained pre-failure manipulator. The computed fault-tolerant workspace is shown in black and has an area of 3.56 sq. units. The artificial joint limits are $[\pm 18, \pm 111, \pm 111]^T$
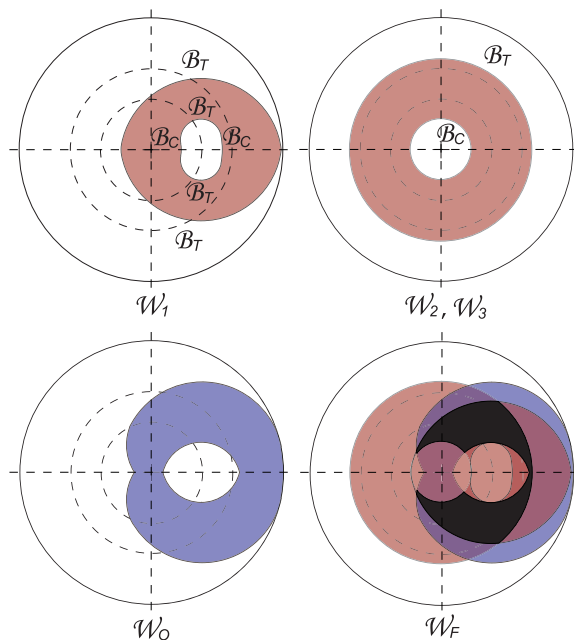

Fig. 7. The optimal fault-tolerant workspace for a 3-DOF planar robot with unequal link lengths. The optimal $\mathcal{W}_F$ is shown in black and has an area of 3.71 sq. unites. The corresponding link lengths are $\mathbf{L} = [1.2, 0.6, 1.2]^T$ units with symmetric artificial joint limits of $[\pm 11, \pm 128, \pm 128]$ degrees.

REFERENCES

[1] E. C. Wu, J. C. Hwang, and J. T. Chladek, "Fault-tolerant joint development for the space shuttle remote manipulator system: Analysis and experiment," *IEEE Trans. Robot. Automat.*, vol. 9, no. 5, pp. 675-684, Oct. 1993.

[2] R. Colbaugh and M. Jamshidi, "Robot manipulator control for hazardous waste-handling applications," *J. Robot. Syst.*, vol. 9, no. 2, pp. 215-250, 1992.

[3] S. Tosunoglu and V. Monteverde, "Kinematic and structural design assessment of faul-tolerant manipulators," *Intell. Automat. Soft Comput.*, vol. 4, no. 3, pp. 261–268, 1998.

[4] B. S. Dhillon and A. R. M. Fashandi, "Safety and reliability assessment techniques in robotics," *Robotica*, vol. 15, no. 6, pp. 701–708, Nov.-Dec. 1997.

[5] C. Carreras and I. D. Walker, "Interval methods for fault-tree analysis in robotics," *IEEE Trans. Robot. Automat.*, vol. 50, no. 1, pp. 3–11, Mar. 2001.

[6] Y. Ting, S. Tosunoglu, and D. Tesar, "A control structure for fault-tolerant operation of robotic manipulators," in *Proc. IEEE Int. Conf. Robot. Automat.*, Atlanta, GA, May 2-6 1993, pp. 684–690.

[7] S. K. Ralph and D. K. Pai, "Computing fault tolerant motions for a robot manipulator," in *Proc. IEEE Int. Conf. Robot. Automat.*, Detroit, MI, May 10-15 1999, pp. 486–493.

[8] J. Park, W.-K. Chung, and Y. Youm, "Failure recovery by exploiting kinematic redundancy," in *Proc. 5th Int. Workshop Robot Human Commun.*, Tsukuba, Japan, Nov. 11-14 1996, pp. 298–305.

[9] Y. Yi, J. E. McInroy, and Y. Chen, "Fault tolerance of parallel manipulators using task space and kinematic redundancy," *IEEE Trans. Robotics*, vol. 22, no. 5, pp. 1017 - 1021, Oct. 2006.

[10] C. J. J. Paredis and P. K. Khosla, "Designing fault-tolerant manipulators: How many degrees of freedom?," *Int. J. Robot. Res.*, vol. 15, no. 6, pp. 611-628, Dec. 1996.

[11] C. L. Lewis and A. A. Maciejewski, "Fault tolerant operation of kinematically redundant manipulators for locked joint failures," *IEEE Trans. Robot. Automat.*, vol. 13, no. 4, pp. 622-629, Aug. 1997.

[12] J. W. Burdick, "On the inverse kinematics of redundant manipulators: Characterization of the self-motion manifolds," in *Proc. IEEE Int. Conf. Robot. Automat.*, Scottsdale, AZ, May 14-19, 1989, pp. 264-270.

[13] C. Lück, "Self-motion representation and global path planning optimization for redundant manipulators through topology-based discretization," *J. Intel. Rob. Syst.*, vol. 19, no. 1, pp. 23-38, May 1997.

[14] R. G. Roberts, "The dexterity and singularities of an underactuated robot," *J. Robotic Syst.*, vol. 18, no. 4, pp. 159-169, 2001.